




Radiomics of Dynamic Contrast-Enhanced MRI for Predicting Radiation-Induced Hepatic Toxicity After Intensity Modulated Radiotherapy for Hepatocellular Carcinoma: A Machine Learning Predictive Model Based on the SHAP Methodology

Fushuang Liu*, Lijun Chen*, Qiaoyuan Wu, Liqing Li , Jizhou Li , Tingshi Su, Jianxu Li, Shixiong Liang , Liping Qing

Department of Radiation Oncology, Guangxi Medical University Cancer Hospital, Nanning, 530001, People's Republic of China

*These authors contributed equally to this work

Correspondence: Shixiong Liang; Liping Qing, Department of Radiation Oncology, Guangxi Medical University Cancer Hospital, 71 he-Di Road, Nanning, 530001, People's Republic of China, Tel +8613917716605; +8615777191169, Email liangshixionglsx@163.com; 371205428@qq.com

Objective: To develop an interpretable machine learning (ML) model using dynamic contrast-enhanced magnetic resonance imaging (DCE-MRI) radiomic data, dosimetric parameters, and clinical data for predicting radiation-induced hepatic toxicity (RIHT) in patients with hepatocellular carcinoma (HCC) following intensity-modulated radiation therapy (IMRT).

Methods: A retrospective analysis of 150 HCC patients was performed, with a 7:3 ratio used to divide the data into training and validation cohorts. Radiomic features from the original MRI sequences and Delta-radiomic features were extracted. Seven ML models based on radiomics were developed: logistic regression (LR), random forest (RF), support vector machine (SVM), eXtreme Gradient Boosting (XGBoost), adaptive boosting (AdaBoost), decision tree (DT), and artificial neural network (ANN). The predictive performance of the models was evaluated using receiver operating characteristic (ROC) curve analysis and calibration curves. Shapley additive explanations (SHAP) were employed to interpret the contribution of each variable and its risk threshold.

Results: Original radiomic features and Delta-radiomic features were extracted from DCE-MRI images and filtered to generate Radiomics-scores and Delta-Radiomics-scores. These were then combined with independent risk factors (Body Mass Index (BMI), V5, and pre-Child-Pugh score(pre-CP)) identified through univariate and multivariate logistic regression and Spearman correlation analysis to construct the ML models. In the training cohort, the AUC values were 0.8651 for LR, 0.7004 for RF, 0.6349 for SVM, 0.6706 for XGBoost, 0.7341 for AdaBoost, 0.6806 for Decision Tree, and 0.6786 for ANN. The corresponding accuracies were 84.4%, 65.6%, 75.0%, 65.6%, 71.9%, 68.8%, and 71.9%, respectively. The validation cohort further confirmed the superiority of the LR model, which was selected as the optimal model. SHAP analysis revealed that Delta-radiomics made a substantial positive contribution to the model.

Conclusion: The interpretable ML model based on radiomics provides a non-invasive tool for predicting RIHT in patients with HCC, demonstrating satisfactory discriminative performance.

Keywords: radiation-induced hepatic toxicity, radiomics, hepatocellular carcinoma, MRI, machine learning

Introduction

Hepatocellular carcinoma (HCC) is one of the most common malignant tumors worldwide, which poses a significant threat to human health.¹ The etiology of HCC has been demonstrated by relevant studies to be closely associated with viral hepatitis,

aflatoxins, hepatic fibrosis, genetic elements, and specific chemical carcinogens.²⁻⁴ Early-stage HCC typically presents with subtle or no clinical symptoms. Studies have demonstrated that approximately 70%-85% of HCC patients are diagnosed at an advanced stage, missing the optimal surgical opportunity.^{5,6} Radiation therapy (RT), which is regarded as one of the key modalities in modern cancer treatment, plays a crucial role in the comprehensive treatment of HCC, particularly in patients with inoperable HCC or those requiring adjuvant therapy (eg, positive surgical margins, portal vein tumor thrombosis).^{4,7,8} With advancements in RT techniques, including intensity-modulated radiation therapy (IMRT), an increasing number of HCC patients have demonstrated effective disease control post-treatment.⁹

However, radiation-induced hepatic toxicity (RIHT), a common dose-limiting factor during RT for HCC patients, has become a significant barrier to treatment efficacy and patient prognosis.¹⁰ Traditionally, the prediction of RIHT has been mainly dependent on clinical factors and dose - volume parameters, such as the patient's age, liver function status, tumor volume, and the irradiated liver dose.¹¹⁻¹³ However, the accuracy of predicting RIHT based on these factors is limited and cannot meet the needs of clinical precision treatment. Gradually, radiomics has been drawing the attention of researchers, which involves extracting and comprehensively analyzing various imaging features to subsequently achieve the quantitative characterization of diseases has been attracting the attention of researchers, which involves the extraction and comprehensive analysis of various imaging features to achieve the subsequent quantitative characterization of diseases.¹⁴ Shen et al found that computed tomography (CT) - based radiomics could predict radiation - induced liver disease in hepatocellular carcinoma patients receiving stereo - tactic body radiotherapy.¹⁵ Unlike traditional static imaging (CT and magnetic resonance imaging(MRI)), which focuses on anatomical structures, dynamic contrast-enhanced magnetic resonance imaging (DCE-MRI) provides a multi-parameter and multi-dimensional evaluation of the liver, enhancing the quantification of anatomical and functional abnormalities,¹⁶ DCE-MRI focuses on microstructural details. Its triphasic dynamic characteristics combined with the temporal analysis advantages of delta-radiomics offer a novel approach for noninvasively predicting the risk of radiation-induced liver injury. This approach has been validated in preoperative evaluations, including assessing vessels encapsulating tumor clusters (VETC) patterns,¹⁷ predicting microvascular invasion¹⁸ and liver function in chronic hepatitis B patients.¹⁹ The typical pathological manifestation of radiation-induced liver injury is hepatic veno-occlusive disease (VOD), characterized by swelling of central venous endothelial cells in the liver lobules, luminal stenosis or obstruction, along with hepatic sinusoid congestion, fibrin deposition, and collagen fiber proliferation, ultimately leading to portal hypertension and hepatic fibrosis.^{20,21} By integrating temporal components and radiomic features, DCE-MRI captures the dynamic distribution changes of contrast agents over time,²² allowing for the quantification of hepatocellular functional impairment²³ and microvascular permeability abnormalities in liver tissue.²⁴ This is closely related to the three mechanisms of radiation-induced liver injury: inflammatory amplification,²⁵ increased oxidative stress, and accelerated fibrosis.^{21,26} This further highlights the unique value of DCE-MRI in liver disease assessment. Machine learning (ML), an important branch of artificial intelligence, has demonstrated its advantages in the diagnosis and treatment of liver cancer.^{27,28} However, these models usually lack high interpretability. Especially in the clinical environment, doctors need to be able to understand and trust the prediction results of the models.

To date, there have been no reports on the use of DCE-MRI models to predict RIHT following radiotherapy. In this study, we aim to develop an interpretable machine learning prediction model that integrates DCE-MRI radiomic features, clinical factors, and dose-volume parameters to predict the occurrence of RIHT. The design objective of this model is to provide evidence for personalized radiotherapy strategies to improve treatment efficacy and ensure patient safety.

Methods and Materials

Patients

Medical records of 481 HCC patients treated with IMRT in the Guangxi Medical University Cancer Hospital between February 2016 and August 2021 were retrospectively reviewed. Finally, after applying the eligibility and exclusion criteria, 150 patients with HCC were enrolled in this study. The patients were diagnosed with HCC histologically and/ or radiologically based on the guidelines of the American Association for the Study of Liver Diseases²⁹ and staged according to the Barcelona Clinic Liver Cancer (BCLC) system.⁸ The inclusion criteria were as follows: (1) Child-Pugh(CP)-A or -B class; (2) Eastern Cooperative Oncology Group (ECOG) scores of 0-2; (3) DCE-MRI images within two weeks prior to IMRT available for the analysis of radiomic features; (4) recovery of all hepatotoxic conditions of patients to grade 1 or less before the first fraction of

radiotherapy in those who received prior interventional therapy and (5) complete follow-up information. The exclusion criteria were as follows: (1) liver metastases and other pathological types of liver tumors and (2) RT interruption.

Radiation Treatment

All patients underwent enhanced CT with a slice thickness of 2.5–5 mm for IMRT planning. To identify intrahepatic lesions, CT and MRI fusion was performed, and all target volumes and critical organs were contoured using MIM software (version 6.8; MIM, USA). The gross tumor volume (GTV) was defined as the tumor lesion. To compensate for organ motion and positioning errors, the planning target volume (PTV) included the GTV plus a safety margin of 5–10 mm in all directions. The tumor irradiation dose, the tolerance dose of the surrounding normal tissues, and the radiotherapy technique used were comprehensively considered,^{30,31} a linear accelerator (6 MV X-ray, ELEKTA Versa-HD or ELEKTA Synergy, Sweden) was used for radiotherapy with a total dose of 45–60 Gy, administered in 15–30 fractions.

Patient Follow-Up and Definition of RIHT

All patients underwent follow-up visits 1–4 months after IMRT completion and subsequently every 3 months, including liver function tests, abdominal dynamic CT, and/or MRI scans, to assess treatment outcomes and side effects. For patients with disease progression, salvage or palliative treatment was provided.

Classic radiation-induced liver disease (RILD) was defined as an anicteric elevation in alkaline phosphatase levels of at least twofold the upper normal level of RILD that occurred between two weeks and three months after RT. Meanwhile, non-classic RILD was defined as elevated levels of liver transaminases (alanine aminotransferase (ALT) or aspartate aminotransferase (AST)) of at least fivefold the upper limit of normal that occurred between one week and three months after RT.³² The evaluation of radiation-induced hepatotoxicity relied on the Child-Pugh scoring system. A Child-Pugh score ($CP \geq 1$ or $CP \geq 2$) is considered an effective tool for assessing radiation-induced hepatotoxicity.

MR Imaging Acquisition

All patients underwent IMRT treatment within two weeks after enhanced MRI examination, using a 1.5-T MRI system to scan the entire liver. Image acquisition was achieved through intravenous injection of Gd-EOB-DTPA (Primovist, Bayer, Germany). Scanning was performed at 20 seconds, 60 seconds, and 180 seconds post-injection to obtain arterial phase, portal venous phase, and delayed phase images (arterial phase (AP), portal venous phase (VP), and delayed phase (DP)). T2-weighted imaging (T2WI) and diffusion-weighted imaging (DWI) sequences were excluded from the radiomic feature analysis due to their slice thickness of approximately 6–10 mm, which may influence the quantitative analysis of radiomic features and were likely to introduce more partial volume effects.^{33,34} Detailed MRI sequences can be found in the [Supplementary Material, Table S1](#).

Radiomics Feature Extraction and Selection

The regions of interest (ROIs) in the AP, VP, and DP of DCE-MRI were manually delineated by two independent radiologists using the MIM software. The ROIs were defined as normal liver tissue, and its extent was the total liver volume minus the GTV, the cystic part, and the gallbladder part. Feature extraction was performed using the FAE software (version 0.5.2; <https://github.com/salan668/FAE>), an open-source software based on PyRadiomics.³⁵ Feature calculation was performed under the condition of resampling to voxel dimensions of $1 \times 1 \times 1 \text{ mm}^3$, and all features conformed to the definitions specified by the Imaging Biomarker Standardization Initiative. A total of 107 features, the detailed descriptions of each feature can be found online (<https://pyradiomics.readthedocs.io/en/latest/features.html>), including first-order features, shape features, texture features, gray-level co-occurrence matrix (GLCM), gray-level dependence matrix (GLDM), gray-level run-length matrix (GLRLM), gray-level size-zone matrix (GLSZM), and neighborhood gray-tone difference matrix (NGTDM), were extracted from each set of images (including original and derived images). The original radiomic features were defined as the image features extracted from three different sequences (AP, PP, and DP). Delta radiomic features were defined as the radiomic matrix data that is obtained by having the radiomic matrix data extracted from images configured at different time points and then being subjected to difference processing ($V - A$, $D - A$, $D - V$).

The reproducibility of the features was evaluated using the intraclass correlation coefficient (ICC). Only the features with an $ICC \geq 0.75$ were retained for subsequent analysis, and the extracted features were normalized using the z-score

method. Redundant and irrelevant features were eliminated using the Pearson correlation coefficient (PCC) with a value of > 0.7 . Subsequently, the least absolute shrinkage and selection operator algorithm (LASSO) was applied. The optimal weight parameter λ was selected using the 5-fold cross-validation method. The radiomics signature was constructed based on these selected features, and the original radiomics scores (Radiomics-scores) and Delta radiomics scores (Delta-Radiomics-scores) were calculated by summing up the weighted coefficients.

Model Construction

Patients were divided into training and validation sets in a 7:3 ratio. Univariate and multivariate logistic regression models were used to identify independent clinical and dosimetric risk factors for RIHT. Subsequently, Spearman correlation analysis was performed by combining the original radiomic scores (Radiomics-scores), Delta radiomic scores (Delta-Radiomics-scores), and independent predictors to assess the strength of the associations between these variables.

The training set patients were split into 70% for training and 30% for internal validation to avoid overfitting, with the internal validation dataset also used for model testing. Independent risk factors, combined with the Radiomics-scores and Delta-Radiomics-scores, were included in the development of the predictive model.

Seven machine learning models were constructed in this study, including logistic regression (LR), random forest (RF), support vector machine (SVM), eXtreme Gradient Boosting (XGBoost), adaptive boosting (AdaBoost), decision tree (DT), and artificial neural network (ANN), for predicting radiation-induced hepatotoxicity. Grid search was used to optimize the hyperparameters of each model, and five-fold cross-validation was employed for hyperparameter selection.

The performance of the models was evaluated using multiple metrics, including comparing the models' area under the curves (AUCs) with the DeLong test, and calculating accuracy, sensitivity, specificity, positive predictive value (PPV), and negative predictive value (NPV) using the critical value determined by the Youden index. The final model was independently tested on the validation set to ensure its generalizability.

Model Interpretation

Shapley additive explanation (SHAP) is a model interpretation framework based on cooperative game theory, with the core idea of quantifying the marginal contribution of each feature to the model's prediction, addressing the interpretability problem of machine learning models.³⁶ This method calculates Shapley values (a fair allocation criterion for feature contributions) to reveal the global impact of features on prediction outcomes, while also analyzing the prediction logic of individual samples at the local level, providing a dual perspective for explaining the "black-box" decision-making of the model.

In this study, the SHAP method was used to provide multi-level interpretation of the optimal model: First, global feature importance ranking (SHAP feature importance) was used to identify key predictors; second, SHAP summary plots were used to visualize the relationship between feature values and prediction directions (promotion/inhibition); finally, clinical significance was combined to select typical cases to construct SHAP force plots, visually demonstrating the positive and negative influences of features in individualized prediction. All analyses were conducted using the SHAP package on the Python platform (Version: 0.46.0).

Statistical Analysis

The cutoff values for continuous laboratory variables were determined using X-tile program 3.6.1 (Chicago, Rim Lab). Continuous variables were expressed as median and interquartile range (IQR), while categorical variables were expressed as frequency and percentage. The clinical characteristics of the training and testing sets were compared using the chi-square test (Chi-square test) and Mann–Whitney *U*-test, respectively. All statistical analyses were performed using R (version 4.2.3; <https://www.r-project.org>), Python (3.10.16), and SPSS 26.0 (IBM Corporation, Armonk, NY). A two-sided *P* value < 0.05 was considered statistically significant for all analyses.

Results

Patient Characteristics

According to the inclusion and exclusion criteria, 150 patients were included in this study. In the entire cohort, the median age was 55 years (IQR, 43–66 years), with 15 females (24.4%) and 135 males (75.6%). Among the patients, 109 (72.6%) were infected with hepatitis B virus (HBV). The median follow-up time was 180 days (IQR, 90–180 days). At the last follow-up, 72 patients (48.0%) experienced RIHT ≥ 1 , and 21 patients (14.0%) experienced RIHT ≥ 2 . Patients were randomly divided (7:3) into the training cohort (106 cases) and the validation cohort (44 cases). There were no significant differences between the training and validation cohorts in factors such as body mass index (BMI), pre-CP score, dose–volume parameters, and the number of people infected with HBV DNA ($P > 0.05$), with baseline characteristics shown in [Tables 1 and 2](#).

Establishment of Radiomics-Scores and Delta-Radiomics-Scores

According to the “Radiomics Feature Extraction and Selection” process described in Radiomics Feature Extraction and Selection, 107 radiomic features were extracted from AP, PP, and DP for the original images, and 107 radiomic features were generated from V-A, D-A, and D-V for the Delta radiomic features. After applying ICC ≥ 0.75 , z normalization, PCC redundancy elimination, and LASSO regression ([Figure 1](#)), a total of three radiomic features for the original images ([Supplementary Material Figure S1A](#)) were identified: AP-original_firstorder_90Percentile, AP-original_firstorder_Variance, and AP-original_glcM_MCC. Additionally, four Delta radiomic features ([Supplementary Material Figure S1B](#)) were identified: DP-VP-

Table 1 Baseline Tables for Total Cohort, Training Cohort, and Validation Cohort

Variables		Total Cohort (N = 150)	Training Cohort (N = 106)	Validation Cohort (N = 44)	P
CP ≥ 1	No	78(52.0%)	58 (54.7%)	20 (45.5%)	0.301
	Yes	72(48.0%)	48 (45.3%)	24 (54.5%)	
CP ≥ 2	No	129(86.0%)	92 (86.8%)	37 (84.1%)	0.664
	Yes	21(14.0%)	14 (13.2%)	7 (15.9%)	
Gender	Male	135(90.0%)	95 (89.6%)	40 (90.9%)	1
	Female	15(10.0%)	11 (10.4%)	4 (9.1%)	
HBV	Negative	41(27.3%)	29 (27.4%)	12 (27.3%)	0.991
	Positive	109(72.7%)	77 (72.6%)	32 (72.7%)	
Cirrhosis	No	84(56.0%)	57 (53.8%)	27 (61.4%)	0.394
	Yes	66(44.0%)	49 (46.2%)	17 (38.6%)	
pre_CP	≤ 6	122(81.3%)	86 (81.1%)	36 (81.8%)	0.922
	> 6	28(18.7%)	20 (18.9%)	8 (18.2%)	
ECOG	0	27(18.0%)	17 (16%)	10 (22.7%)	0.332
	1/2	123(82.0%)	89 (84.0%)	34 (77.3%)	
BCLC_stage	A	36(24.0%)	24 (22.6%)	12 (27.3%)	0.796
	B	16(10.7%)	11 (10.4%)	5 (11.4%)	
	C	98(65.3%)	71 (67%)	27 (61.4%)	
Lymph_node_metastasis	No	125(83.3%)	87 (82.1%)	38 (86.4%)	0.521
	Yes	25(16.7%)	19 (17.9%)	6 (13.6%)	
Distant_metastasis	No	124(82.7%)	88 (83%)	36 (81.8%)	0.860
	Yes	26(17.3%)	18 (17%)	8 (18.2%)	
Vascular_cancer_thrombosis	No	95(63.3%)	64 (60.4%)	31 (70.5%)	0.244
	Yes	55(26.7%)	42 (39.6%)	13 (29.5%)	
Age	≤ 55	77(51.3%)	52 (49.1%)	25 (56.8%)	0.387
	> 55	73(48.7%)	54 (50.9%)	19 (43.2%)	
AST, u/l	≤ 40	83(55.3%)	59 (55.7%)	24 (54.5%)	0.900

(Continued)

Table 1 (Continued).

Variables		Total Cohort (N = 150)	Training Cohort (N = 106)	Validation Cohort (N = 44)	P
ALT, u/l	>40	67(44.7%)	47 (44.3%)	20 (45.5%)	0.206
	≤40	87(58.0%)	58 (54.7%)	29 (65.9%)	
ALP, u/l	>40	63(42.0%)	48 (45.3%)	15 (34.1%)	0.337
	≤150	115(76.7%)	79 (74.5%)	36 (81.8%)	
AFP, ng/mL	>150	35(23.3%)	27 (25.5%)	8 (18.2%)	0.069
	<400	111(74.0%)	74 (69.8%)	37 (84.1%)	
Tumor_size, cm	≥400	39(26.0%)	32 (30.2%)	7 (15.9%)	0.175
	≤5	59(39.3%)	38 (35.8%)	21 (47.7%)	
Immune checkpoint inhibitor therapy	>5	91(60.7%)	68 (64.2%)	23 (52.3%)	0.339
	No	135(90.0%)	97(91.5%)	38(86.1%)	
Targeted therapy	Yes	15(10.0%)	9(8.5%)	6(13.6%)	0.410
	No	139(92.7%)	99(93.4%)	40(90.9%)	
	Yes	11(7.3%)	7(6.6%)	4(9.1%)	

Note: Both cohorts were well balanced in the clinical characteristics. Statistical comparisons between the training and validation cohorts were computed using the χ^2 test.

Abbreviations: HBV, Hepatitis B Virus; ECOG, Eastern Cooperative Oncology Group; AST, Aspartate aminotransferase; ALT, Alanine aminotransferase; ALP, Alkaline phosphatase; AFP, Alpha - fetoprotein; BCLC, Barcelona clinic liver cancer; CP, Child–Pugh.

Table 2 Dose–Volume Parameters Baseline Tables for Training Cohort and Validation Cohort

Variables	Training Cohort Median (IQR)	Validation Cohort Median (IQR)	P
Dose, Gy	51.00 (48.00–60.00)	50.30 (50.00–60.00)	0.939
GTV volume, mL	185.13 (75.11–611.21)	161.45 (53.68–606.62)	0.561
Normal liver volume, mL	982.30 (773.34–1173.40)	942.73 (759.73–1147.85)	0.898
Dmean, cGy	1756.70 (1344.50–2112.03)	1793.50 (1278.80–2060.78)	0.904
V5, %	66.31 (55.47–81.06)	72.55 (59.28–82.13)	0.391
V10, %	49.92 (36.88–60.31)	55.099 (36.79–63.58)	0.501
V15, %	39.67 (28.79–50.04)	44.78 (29.21–52.09)	0.426
V20, %	33.65 (22.60–42.87)	36.08 (23.34–44.24)	0.543
V25, %	29.20 (19.45–37.25)	30.15 (18.43–38.38)	0.659
V30, %	24.26 (15.64–30.49)	25.21 (14.52–31.72)	0.814
V35, %	19.60 (11.91–25.61)	20.29 (11.06–25.34)	0.787
Vs5, mL	298.15 (166.11–413.20)	287.66 (169.83–373.28)	0.686
Vs10, mL	462.56 (324.05–603.11)	446.04 (316.07–580.87)	0.686
Vs15, mL	549.91 (446.48–695.99)	548.17 (431.57–665.87)	0.760
Vs20, mL	606.65 (502.62–767.78)	621.89 (515.99–767.52)	0.875
Vs25, mL	672.41 (559.42–849.30)	687.28 (550.18–796.01)	0.875
Vs30, mL	717.50 (595.56–909.81)	748.65 (611.73–844.74)	0.905
Vs35, mL	761.16 (621.99–955.29)	795.709 (625.49–910.94)	0.931
BMI, kg/m ²	22.50 (20.01–24.70)	21.75 (20.00–23.50)	0.381

Note: Both cohorts were well balanced in the dose–volume parameters variables. Statistical comparisons between the training and validation cohorts were computed using the Wilcoxon test.

Abbreviations: IQR, interquartile range; GTV, gross tumor volume; Dmean, mean dose; BMI, body mass index; Vx, the percentage (%) of normal liver volume receiving more than x Gy; Vsx, the volume of normal liver receiving more than xGy.

original_glszm_LargeAreaHighGrayLevelEmphasis, DP-AP-original_shape_VoxelVolume, DP-AP-original_gldm_DependenceNonUniformity, and DP-AP-original_gldm_DependenceVariance. Subsequently, Radiomics-scores and Delta-Radiomics-scores were constructed.

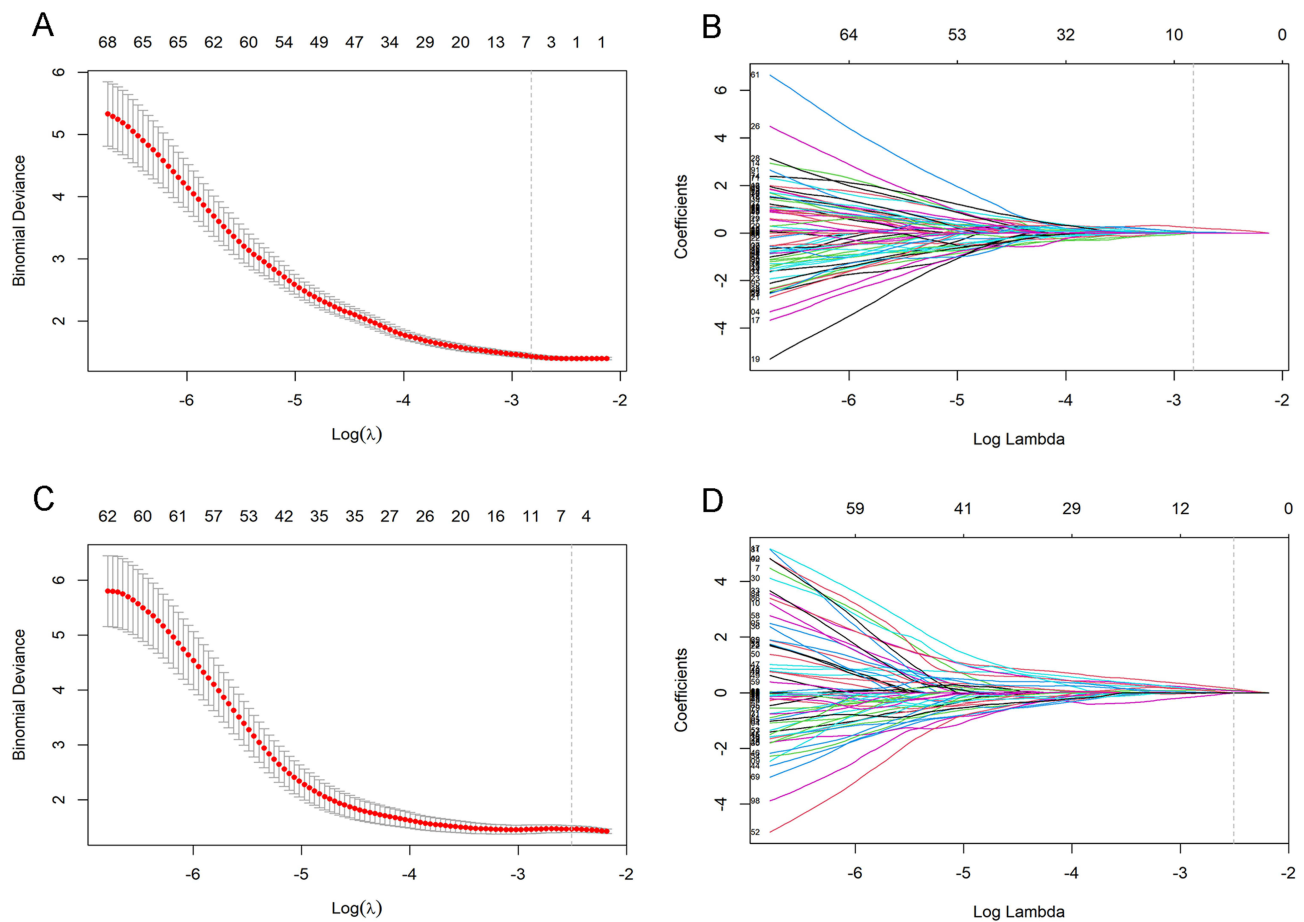


Figure 1 Radiomics feature selection using the LASSO regression analysis. (A) and (B) is the original radiomic features; (C) and (D) is the delta radiomic features.

Model Performance

The univariate and multivariate logistic regression analyses of the training cohort for predicting the outcomes associated with $\text{RIHT} \geq 1$ are presented in Table 3. The results of the univariate logistic analysis showed that BMI, pre_CP, Dmean, V5-35, and Vs5-25 were significantly associated with $\text{RIHT} \geq 1$ ($P < 0.05$). The multivariate logistic regression analysis indicated that BMI (OR: 0.582, 95% CI: 0.378–0.896, $P = 0.014$), pre_CP (OR: 4.478, 95% CI: 1.166–17.194, $P = 0.029$), V5 (OR: 1.75, 95% CI: 1.108–2.763, $P = 0.016$), and Vs5 (OR: 1.062, 95% CI: 1.014–1.113, $P = 0.011$) were independent risk factors for $\text{RIHT} \geq 1$. Spearman correlation analysis was conducted using Radiomics-scores, Delta-Radiomics-scores, and independent predictive factors (BMI, pre_CP, V5, and Vs5). According to the Spearman correlation analysis (Figure 2), a strong negative correlation ($\rho = -0.86$) was observed only between Vs5 and V5. V5 demonstrated greater interpretability in clinical applications, and thus, Vs5 was excluded. The correlations between the remaining variables were generally weak. Specifically, the correlation coefficients between Radiomics_Score, Delta_Radiomics_Score, V5, and BMI were all less than or equal to 0.23, indicating a weak association. Subsequently, models were constructed using LR, RF, SVM, XGBoost, AdaBoost, DT, and ANN. The Supplementary Material lists the optimal hyperparameters for each model. External validation was then performed.

The performance of the ML models in the training and test cohorts is shown in Table 4. In the training cohort, the AUC values were 0.8651 (95% Confidence interval (CI): 0.7182–0.9798) for LR, 0.7004 (95% CI: 0.5159–0.8651) for RF, 0.6349 (95% CI: 0.4008–0.8300) for SVM, 0.6706 (95% CI: 0.4682–0.8413) for XGBoost, 0.7341 (95% CI: 0.5431–0.8981) for AdaBoost, 0.6806 (95% CI: 0.4960–0.8552) for DT, and 0.6786 (95% CI: 0.4726–0.8500) for ANN. The results of the Delong test indicated that LR showed a significant difference in AUC compared to RF ($P = 0.024$), SVM ($P = 0.026$), XGBoost ($P = 0.021$), DT ($P = 0.020$), and ANN ($P = 0.034$), whereas no significant

Table 3 Univariate and Multivariable Logistic Regression Analysis of the Risk Factors in the Training Cohort

Variables	Univariate Analysis		Multivariate Analysis	
	OR (95% CI)	P	OR (95% CI)	P
Gender	2.305(0.632–8.405)	0.206	–	–
Age	1.723(0.796–3.732)	0.168	–	–
HBV	1.244(0.524–2.951)	0.621	–	–
Cirrhosis	0.714(0.33–1.544)	0.392	–	–
ECOG	0.914(0.322–2.591)	0.866	–	–
AFP	0.915(0.397–2.108)	0.835	–	–
Tumor_number	1.012(0.466–2.199)	0.976	–	–
Lymph_node_metastasis	1.108(0.41–2.995)	0.840	–	–
Distant_metastasis	0.729(0.259–2.056)	0.551	–	–
Vascular_cancer_thrombosis	0.997(0.456–2.179)	0.994	–	–
BMI	0.815(0.709–0.936)	0.004*	0.582(0.378–0.896)	0.014*
pre_CP	1.869(1.163–3.005)	0.010*	4.478(1.166–17.194)	0.029*
AST	0.999(0.996–1.002)	0.578	–	–
ALT	0.998(0.994–1.003)	0.492	–	–
ALP	1.001(0.996–1.006)	0.776	–	–
Tumor_size	1.036(0.948–1.131)	0.434	–	–
Dose	1.015(0.967–1.064)	0.551	–	–
GTV_volume	1(0.999–1.001)	0.638	–	–
Normal_liver_volume	1(0.999–1.001)	0.871	–	–
Dmean	1.002(1.001–1.003)	<0.001*	1.005(0.999–1.012)	0.114
V5	1.051(1.023–1.08)	<0.001*	1.75(1.108–2.763)	0.016*
V10	1.052(1.024–1.081)	<0.001*	1.133(0.756–1.7)	0.545
V15	1.062(1.03–1.096)	<0.001*	0.617(0.15–2.537)	0.503
V20	1.077(1.038–1.117)	<0.001*	0.036(0.001–3.398)	0.152
V25	1.093(1.047–1.141)	<0.001*	79.204(0.379–16,538.099)	0.109
V30	1.104(1.052–1.159)	<0.001*	1.118(0.251–4.967)	0.884
V35	1.106(1.049–1.166)	<0.001*	0.449(0.144–1.398)	0.167
Vs5	0.997(0.995–0.999)	0.007*	1.062(1.014–1.113)	0.011*
Vs10	0.997(0.995–0.999)	0.004*	0.999(0.973–1.026)	0.941
Vs15	0.997(0.995–0.999)	0.005*	0.962(0.86–1.077)	0.503
Vs20	0.998(0.996–0.999)	0.012*	0.747(0.509–1.095)	0.134
Vs25	0.998(0.996–1)	0.027*	1.488(0.953–2.323)	0.081
Vs30	0.998(0.997–1)	0.056	–	–
Vs35	0.999(0.997–1)	0.095	–	–

Note: Performed univariate and multivariate analyses using logistic regression analysis. * $P < 0.05$.

Abbreviations: OR, odds ratio; CI, confidence interval; HBV, Hepatitis B Virus; ECOG, Eastern Cooperative Oncology Group; AST, Aspartate aminotransferase; ALT, Alanine aminotransferase; ALP, Alkaline phosphatase; AFP, Alpha -fetoprotein; BCLC, Barcelona clinic liver cancer; CP, Child–Pugh; BMI, body mass index; GTV, gross tumor volume; Dmean, mean dose; Vx, the percentage (%) of normal liver volume receiving more than x Gy; Vsx, the volume of normal liver receiving more than xGy.

difference was observed between LR and AdaBoost ($P = 0.097$) ([Supplementary Material, Table S2](#)). However, compared to XGBoost, LR demonstrated superior accuracy, sensitivity, PPV, and NPV. In the validation cohort, LR (AUC: 0.725) outperformed RF (AUC: 0.595), SVM (AUC: 0.570), XGBoost (AUC: 0.640), AdaBoost (AUC: 0.611), DT (AUC: 0.688), and ANN (AUC: 0.563). The LR model exhibited an accuracy of 0.705, sensitivity of 0.667, specificity of 0.750, PPV of 0.762, and NPV of 0.652 in the validation cohort. Therefore, LR was selected as the final model. Additionally, the receiver operating characteristic (ROC) curves ([Figure 3](#)) and performance radar plots ([Figure 4](#)) for all models in the training and validation cohorts are presented. The calibration curve ([Figure 5](#)) illustrates a good agreement between the predicted probabilities of LR and the actual occurrence of RIHT ≥ 1 in the total cohort.

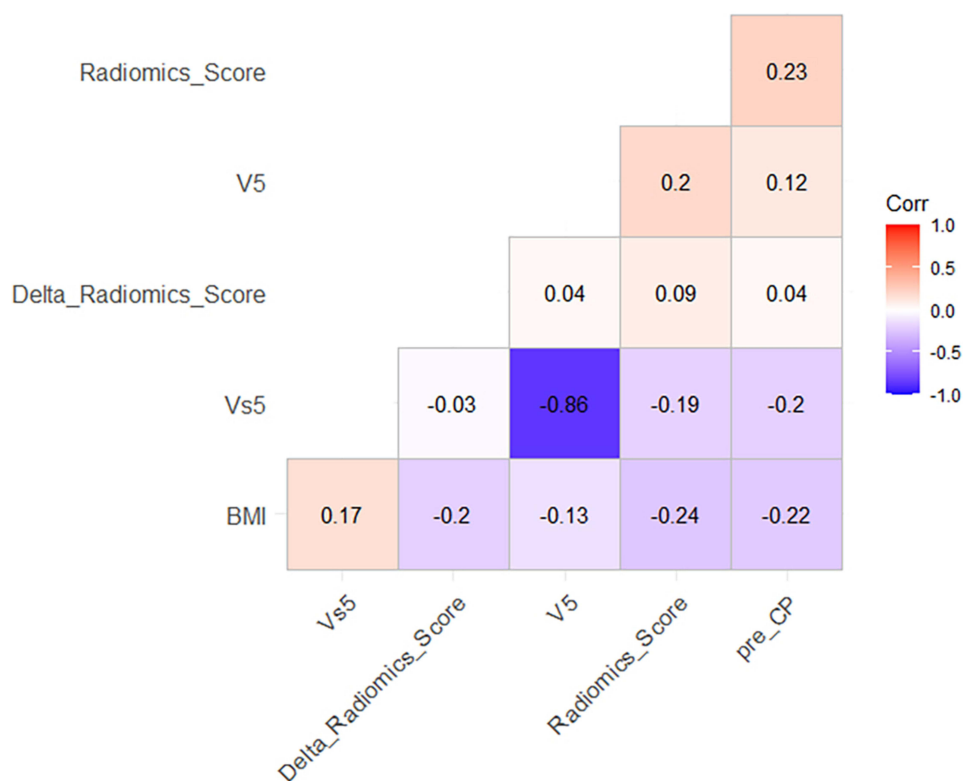


Figure 2 The Spearman rank correlation.

Model Interpretability

SHAP values were calculated for each independent risk factor in the LR model. In the interpretation, the SHAP bar plot (Figure 6A) illustrates the importance of each feature, with the results indicating that Delta_Radiomics contributed the most to the LR model. A summary plot of the SHAP values (Figure 6B) was generated, which explains the impact of

Table 4 Comparison of the Performance of ML Models in Training and Validation Cohorts

Models		AUC	Accuracy	Sensitivity	Specificity	PPV	NPV
Training cohort	LR	0.865	0.844	0.786	0.889	0.846	0.842
	RF	0.700	0.656	0.857	0.500	0.571	0.818
	SVM	0.635	0.750	0.429	1.000	1.000	0.692
	XGBoost	0.671	0.656	0.786	0.556	0.579	0.769
	AdaBoost	0.734	0.719	0.786	0.667	0.647	0.800
	DT	0.681	0.688	0.857	0.556	0.600	0.833
	ANN	0.679	0.719	0.500	0.889	0.778	0.696
Validation cohort	LR	0.725	0.705	0.667	0.750	0.762	0.652
	RF	0.595	0.614	0.417	0.850	0.769	0.548
	SVM	0.570	0.636	0.542	0.750	0.722	0.577
	XGBoost	0.640	0.636	0.417	0.900	0.833	0.563
	AdaBoost	0.612	0.636	0.583	0.700	0.700	0.583
	DT	0.688	0.682	0.625	0.750	0.750	0.625
	ANN	0.563	0.591	0.333	0.900	0.800	0.529

Abbreviations: AUC, area under the curves; LR, Logistic Regression; RF, Random Forest; SVM, Support Vector Machine; XGBoost, eXtreme Gradient Boosting; AdaBoost, Adaptive Boosting; DT, Decision Tree; ANN, and Artificial Neural Network; PPV, positive predictive value; NPV, negative predictive value.

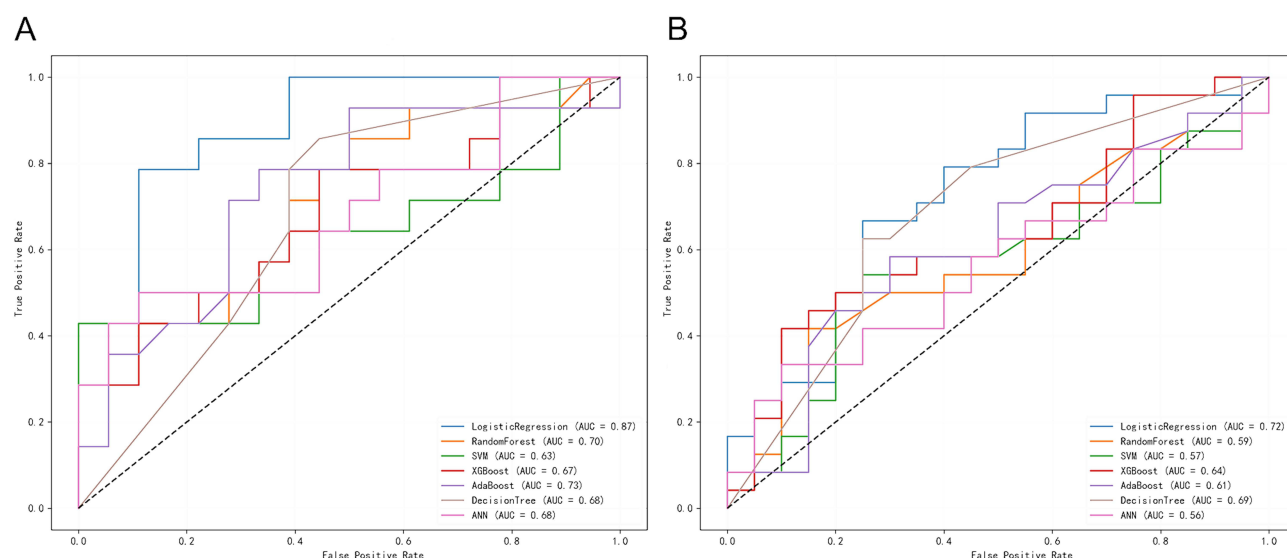


Figure 3 ROC curves of the training and validation cohorts of 7 ML models. **(A)** ROC curves of the training cohort. **(B)** ROC curves of the validation cohort.

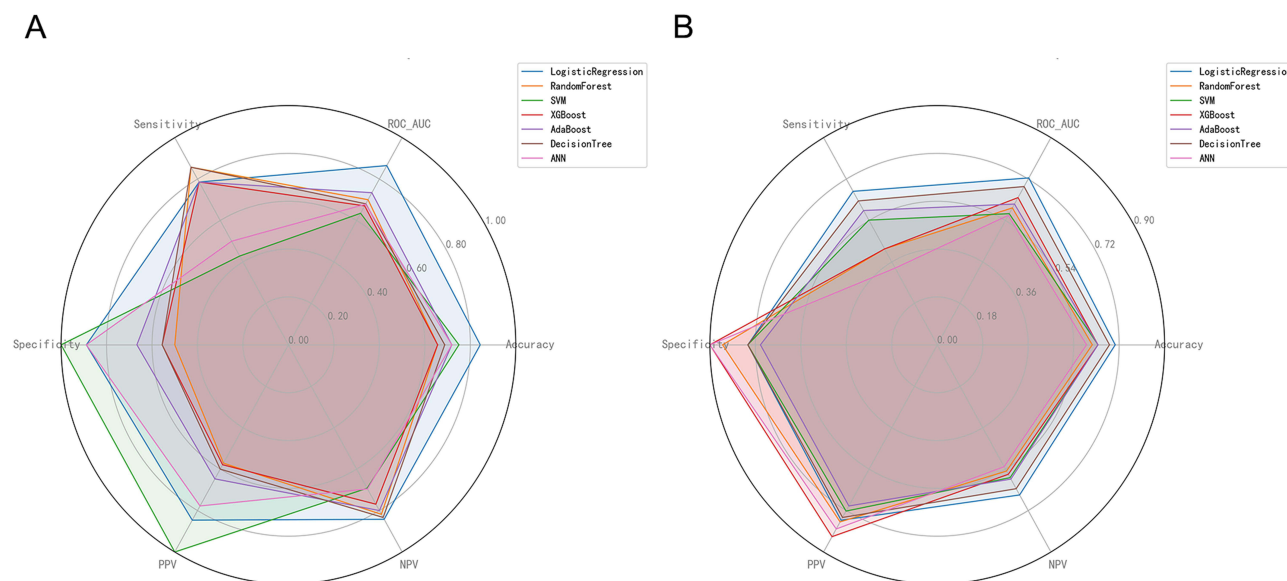


Figure 4 The performance radar chart of the training and validation cohorts of 7 ML models. **(A)** Performance radar chart of the training cohort. **(B)** Performance radar chart of the validation cohort.

each feature on the model's predictions. Furthermore, two typical examples were provided by us to illustrate the interpretability of the model. Figure 7 shows two typical cases correctly predicted as $RIHT \geq 1$ and $RIHT < 1$.

Discussion

In this study, an interpretable ML model was developed to predict RIHT in patients with primary HCC following IMRT. The model utilizes radiomic features extracted from DCE-MRI, clinical parameters, and dosimetric volume parameters, demonstrating promising performance. The radiomic features (Radiomics-scores and Delta-Radiomics-scores), along with BMI, V5, and the pre-CP, reflect critical aspects of liver tissue characteristics and individual patient features, providing key predictive value for the occurrence of RIHT. The LR model exhibited the best performance in both the training cohort (AUC = 0.865) and validation cohort (AUC = 0.725), showing a significant advantage over other machine

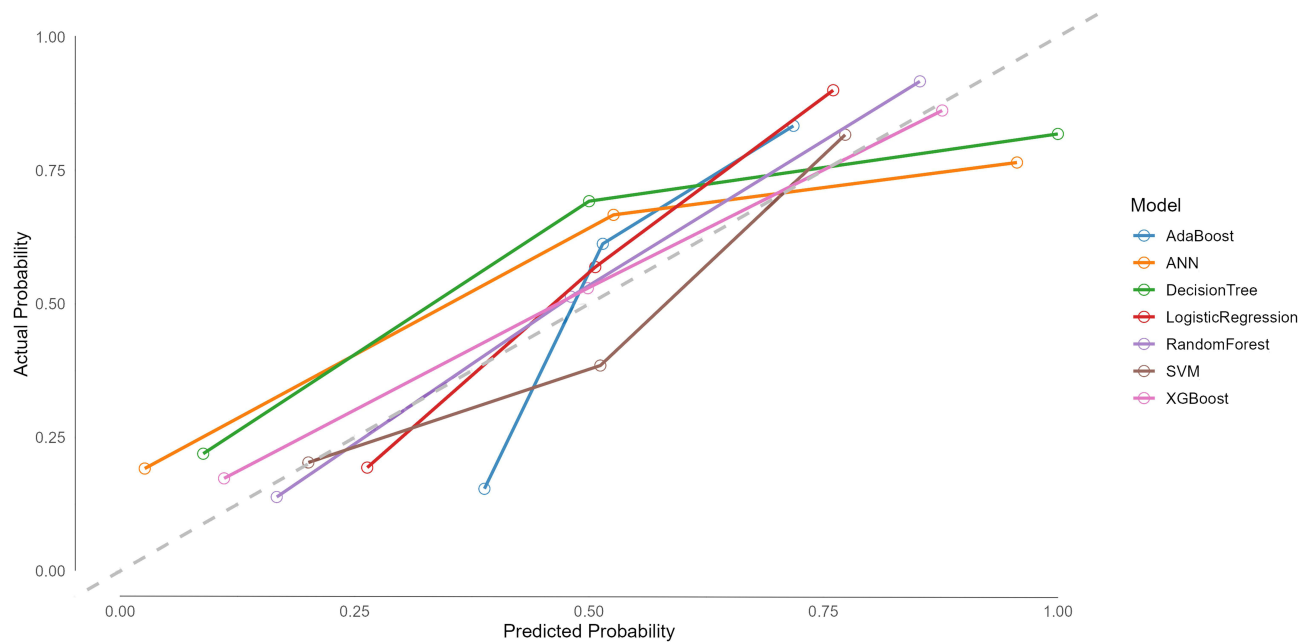


Figure 5 The calibration curve of the all cohort of 7 ML models.

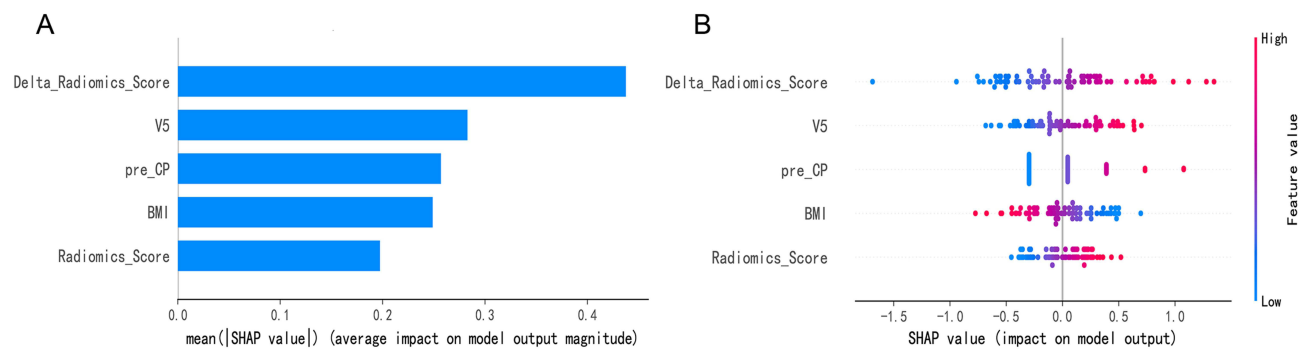


Figure 6 The interpretability of the ML radiomics model was assessed using the SHAP method. **(A)** The SHAP bar chart shows the importance of each feature based on the mean SHAP values. **(B)** The SHAP summary plot shows the impact of each feature on the model predictions. Individual dots symbolize patients, and different colors represent different levels of influence on the model output.

learning algorithms, such as RF and SVM. To the best of our knowledge, this is the first exploratory attempt to construct a non-invasive predictive model for RIHT using DCE-MRI-based radiomic features and interpretable ML algorithms.

RIHT is a dose-limiting toxicity. Previous studies have primarily focused on the mean liver dose (MLD) or V30.^{37,38} In clinical practice, studies on liver radiation tolerance based on three-dimensional conformal radiation therapy (3D-CRT) have suggested that we consider $V5 \leq 86\%$ as the liver dose limit standard,³⁸ and in our patients, V5 did not exceed the threshold. IMRT is a more complex form of conformal radiation therapy, which, compared to previous 3D-CRT, particularly emphasizes strict liver dose-volume constraints. The arrangement of multiple beams in the plan enhances target conformity while increasing the dose gradient.³⁹ In this case, traditional dosimetric parameters may no longer be independent predictors of RIHT. Although strict dose-volume constraints can reduce the variation in dose-volume metrics between individuals, significant differences may still exist in spatial dose distribution. This may be related to the radiation sensitivity of the liver's microvascular network, where diffuse endothelial injury caused by low-dose radiation may amplify liver damage effects through an inflammatory cascade.⁴⁰ V5 is used as an important metric for assessing the extent of liver damage in radiation therapy plans, and its correlation with RIHT has been confirmed by multiple



Figure 7 Force plots of personalized feature attributions of HCC patients with RIHT < 1 (A) and RIHT ≥ 1 (B). The arrow was used to represent contribution of each feature, the arrow pushes either a decrease (negative contribution) or an increase (positive contribution) in outcome probability. The red color indicates positive contribution, while blue color indicates negative contribution. The length of each arrow is proportional to the SHAP value of the feature.

studies,^{38,41} which is consistent with our findings ($P = 0.016$). Therefore, the long-term effects of low-dose radiation need to be reassessed, particularly in patients with coexisting cirrhosis or metabolic syndrome. Even if the MLD is within acceptable limits, extensive low-dose irradiation may still lead to irreversible damage.

The pre-CP is an important indicator for assessing liver function. Wu et al and Su et al developed nomograms based on the pre-CP score to predict RIHT.^{42,43} This study further demonstrated that patients with a Child-Pugh score >6 had a fourfold higher likelihood of developing RIHT than those with a score ≤6 ($P = 0.029$, OR = 4.478, 95% CI: 1.166–17.194). A higher Child-Pugh score indicates more severe hepatic dysfunction, with lower hepatic reserve and metabolic capacity.⁴⁴ This affects the risk of RIHT in HCC patients. BMI is widely recognized as a clinical indicator reflecting nutritional status and metabolic profile.⁴⁵ The malnutrition state associated with low BMI may reduce radiation tolerance in hepatic parenchymal cells, while the underlying pathological mechanisms contributing to BMI reduction, particularly those associated with tumor catabolism, may disrupt systemic homeostasis.^{46,47} This dual-pathway mechanism may impair hepatic metabolic regulation and immune function, thereby indirectly elevating susceptibility to RIHT.

In recent years, radiomics-based image analysis technology has developed rapidly, providing a non-invasive and automated method for tumor diagnosis, staging, and prognosis prediction.¹⁴ Previous studies have shown that pre-treatment CT radiomics models can predict radiation-induced liver injury (AUC = 0.889),¹⁵ which is higher than clinical models (AUC = 0.763).⁴² However, many patients with intermediate or advanced-stage HCC, who undergo transcatheter arterial chemoembolization (TACE) treatment, may develop significant radiological artifacts on CT scans due to the accumulation of iodized oil in radiation-affected areas, which do not appear on MRI. This could lead to misjudgment of the normal liver boundary during radiomics feature extraction using CT images due to radiological artifacts.⁴⁸ Radiomics based on DCE-MRI has also garnered increasing attention, especially due to its superior soft tissue contrast and anti-artifact properties,^{49,50} which facilitate multi-parameter and multi-dimensional liver evaluation. It also enhances the quantitative analysis of anatomical structures and functional abnormalities.¹⁶ Previous studies have demonstrated the successful application of radiomics models based on DCE-MRI in predicting liver diseases.^{17–19} DCE-MRI can reflect functional information such as tissue blood flow, vascular status, and blood perfusion.⁵¹ Kim et al⁵² and Choi et al⁵³ reported that insufficient compensation of hepatic arterial flow can damage the liver parenchyma, causing edema and hepatocytic depletion. This helps assess changes in liver tissue microstructure and function. While delta-radiomics provides information on hemodynamics, original multi-parameter radiomics offers insights into tumor morphology and tissue characteristics. Integrating these two types of information enables a more comprehensive visualization for predicting RIHT.⁵⁴

In this study, the original imaging features, namely AP-original_firstorder_90Percentile and AP-original_firstorder_Variance, reflected the distribution and dispersion of normal liver tissue at higher gray-scale values. This suggests a degree of tissue heterogeneity and microstructural unevenness, which may be associated with local inflammatory reactions in the liver.⁵⁵ The maximum correlation coefficient in the gray-level co-occurrence matrix (AP-original_gldm_MCC) disclosed the linear correlation between different gray levels in liver tissue. It is closely linked to microstructural changes like disordered cell arrangement and increased stroma, which may impact hepatic perfusion and metabolism.⁵⁶ Changes in the delta-radiomics features of gray-level dependence matrix nonuniformity and variance (DP-AP-original_gldm_DependenceNonUniformity and DP-AP-original_gldm_DependenceVariance) reflected the heterogeneity in gray-level dependence and variation during dynamic enhancement. These changes are associated with physiological processes such as hepatic perfusion and vascular permeability.⁵⁷ Changes in the shape feature (DP-AP-original_shape_VoxelVolume) visually demonstrated the dynamic morphological changes in liver tissue. Associated with pathological processes like cellular swelling or atrophy, these changes offer crucial information for assessing liver function.⁵⁸ DP-VP-original_glszm_LargeAreaHighGrayLevelEmphasis reflected the emphasis on large high-gray-value regions. Linked to perfusion differences between the hepatic arterial and portal venous phases, this feature aids in reflecting the hepatic blood supply and microcirculation status.⁵⁹ SHAP analysis, a general tool for assessing feature importance in ML models, was employed to analyze and investigate the contributions of different variables in the risk prediction model. In our study, SHAP analysis revealed delta-radscore as the most informative feature, capturing subtle changes in liver tissue during dynamic enhancement. The information provided by these radiomic features complements conventional imaging findings and is difficult to interpret and identify with the naked eye.^{60,61} Thus, DCE-MRI-based radiomics strongly supports the prevention of radiation-induced liver toxicity.

Among the seven machine learning models, the LR model demonstrated superior performance in both the training and validation groups, confirming that the LR model not only fits well on the training set but also exhibits strong generalization ability when facing new data. Our model outperforms previous studies that used deep learning methods to predict radiation-induced liver injury (AUC: 0.865 vs 0.79).⁶² Although the LR model performed well on both the training and validation sets, the AUC value on the validation set (0.725) was lower than that on the training set (0.865), suggesting a potential overfitting risk. Expanding the sample size is critical for enhancing the model's generalization ability and reducing overfitting. The LR model's sensitivity (0.786) and negative predictive value (0.842) indicate room for improvement. Future model optimization could involve increasing the sample size or incorporating temporal imaging features, such as DCE-MRI data from multiple post-radiotherapy time points. The LR model's linear combination approach quantifies each variable's contribution, aligning with the preference for "white-box models" in clinical settings. While the relationships between data features in this study are relatively simple and linear, differences across datasets in sample size, data distribution, feature dimensions, and relationships require further assessment of the LR model's generalizability using multi-center datasets. However, models like RF, SVM, and XGBoost had relatively low AUC values, indicating potential limitations in their training processes. While these models excel at handling complex data and non-linear relationships, with small sample sizes ($n=150$), the decision tree splitting in RF/XGBoost can capture noise features. This may result from inadequate feature capture or a mismatch between model complexity and data characteristics.⁶³

HCC patients exhibit heterogeneity, necessitating individualized treatment approaches for each patient.⁶⁴ Clinicians can utilize the LR model, integrated with clinical and radiomic data, to develop more targeted radiotherapy plans. For patients with low BMI, limited liver reserve function, and high predicted risk, a multidisciplinary team should be consulted to adjust treatment strategies. Initiate hepatoprotective therapy (eg, bicyclol) to enhance liver tolerance,⁶⁵ increase liver function monitoring, detect early signs of RIHT, and promptly implement interventions such as adjusting radiotherapy doses or temporarily halting treatment to mitigate liver injury. Combining immune checkpoint inhibitors (eg, anti-PD-1 antibodies) or anti-angiogenic agents (eg, lenvatinib) can synergistically enhance antitumor effects and reduce radiotherapy dose requirements.^{66,67}

This study also has several limitations. First, the relatively small sample size and lack of external validation may affect the generalizability and stability of the model. Second, while SHAP was used to explain the model's predictions, further exploration into the mechanisms underlying RIHT is needed, incorporating additional clinical data and biological

markers, such as gene expression and proteomic data, to develop a more accurate predictive model. Finally, the manual segmentation of the ROI by clinicians is time-consuming and may introduce subjectivity and variability. Therefore, future research should focus on advanced deep learning-based automatic segmentation and end-to-end techniques to minimize human intervention, ensuring reproducibility and efficiency.

Conclusion

This study successfully developed a machine learning model based on DCE-MRI radiomics, clinical, and dosimetric parameters, demonstrating the superior performance of the logistic regression model in predicting RIHT. The model not only provides a practical tool for clinical risk assessment of liver toxicity but also offers valuable insights by revealing the role of dynamic imaging features. It enables effective prediction of RIHT following IMRT for primary hepatocellular carcinoma, thereby achieving the goal of “precision toxicity avoidance” in individualized treatment.

Abbreviations

HCC, hepatocellular carcinoma; RT, radiation therapy; IMRT, intensity-modulated radiation therapy; RIHT, radiation-induced hepatic toxicity; DCE-MRI, dynamic contrast-enhanced magnetic resonance imaging; ML, machine learning; BCLC, Barcelona Clinic Liver Cancer; ECOG, Eastern Cooperative Oncology Group; HBV, Hepatitis B virus; AST, aspartate aminotransferase; ALT, alanine aminotransferase; ALP, alkaline phosphatase; AFP, alpha-fetoprotein; BMI, Body Mass Index; CT, computed tomography; GTV, gross tumor volume; PTV, planning target volume; T2WI, T2-weighted imaging; DWI, diffusion-weighted imaging; ROIs, regions of interest; AP, arterial phase; VP, portal venous phase; DP, delayed phase; VOI, volume of interest; GLCM, gray-level co-occurrence matrix; GLDM, gray-level dependence matrix; GLRLM, gray-level run-length matrix; GLSZM, gray-level size-zone matrix; NGTDM, neighborhood gray-tone difference matrix; ICC, intra-observer intraclass correlation coefficient; PCC, Pearson correlation coefficient; LASSO, least absolute shrinkage and selection operator; LR, logistic regression; RF, random forest; SVM, support vector machine; XGBoost, eXtreme Gradient Boosting; AdaBoost, Adaptive Boosting; DT, decision tree; ANN, artificial neural network; RILD, Radiation-induced liver disease; ROC curves, Receiver operating characteristic curves; CI, Confidence interval; AUCs, Area under the curve; PPV, positive predictive value; NPV, negative predictive value; SHAP, Shapley additive explanation; IQR, interquartile range; TACE, transcatheter arterial chemoembolization; MLD, mean liver dose; 3D-CRT, three-dimensional conformal radiation therapy.

Data Sharing Statement

The statistical codes and datasets used and/or analyzed during the current study are available from the corresponding author (371205428@qq.com) on reasonable request.

Ethics Approval

The protocol of this retrospective study conformed to the Declaration of Helsinki (1975) and its amendments and was approved by the Ethics Review Committee of the Guangxi Medical University Cancer Hospital (KY2025593), which waived the requirement for written informed consent because patients or their legal guardians had consented, upon admission, to analysis and publication of anonymized medical data for research purposes.

Acknowledgments

We sincerely appreciate the support and contributions of all the authors to this research and manuscript.

Funding

This research was supported by the Guangxi Medical and Health Key Scientific Research Project (No. Zhong 2010071).

Disclosure

The authors declare no competing interests in this work.

References

- Vogel A, Meyer T, Sapisochin G, et al. Hepatocellular carcinoma. *Lancet*. 2022;400(10360):1345–1362. doi:10.1016/s0140-6736(22)01200-4
- Chen CJ, Yang HI, Su J, et al. Risk of hepatocellular carcinoma across a biological gradient of serum hepatitis B virus DNA level. *JAMA J Am Med Assoc*. 2006;295(1):65–73. doi:10.1001/jama.295.1.65
- Cai PR, Zheng H, She JJ, et al. Molecular mechanism of aflatoxin-induced hepatocellular carcinoma derived from a bioinformatics analysis. *Toxins*. 2020;12(3):203. doi:10.3390/toxins12030203
- Benson AB, D'Angelica MI, Abbott DE, et al. Hepatobiliary cancers, version 2.2021. *J National Compr Cancer Network*. 2021;19(5):541–565. doi:10.6004/jnccn.2021.0022
- Yang C, Zhang HL, Zhang LM, et al. Evolving therapeutic landscape of advanced hepatocellular carcinoma. *Nat Rev Gastroenterol Hepatol*. 2023;20(4):203–222. doi:10.1038/s41575-022-00704-9
- Pang TC, Lam VW. Surgical management of hepatocellular carcinoma. *World J Hepatol*. 2015;7(2):245–252. doi:10.4254/wjh.v7.i2.245
- Kirsch DG, Diehn M, Kesarwala AH, et al. The future of radiobiology. *Jnci-J Nat Cancer Instit*. 2018;110(4):329–340. doi:10.1093/jnci/djx231
- Reig M, Forner A, Rimola J, et al. BCLC strategy for prognosis prediction and treatment recommendation: the 2022 update. *J Hepatol*. 2022;76:681–693. doi:10.1016/j.jhep.2021.11.018
- Li LQ, Zhou Y, Huang Y, et al. Stereotactic body radiotherapy versus intensity-modulated radiotherapy for hepatocellular carcinoma with portal vein tumor thrombosis. *Hepatol Internat*. 2021;15(3):630–641. doi:10.1007/s12072-021-10173-y
- Munoz-Schuffenegger P, Ng S, Dawson LA. Radiation-induced liver toxicity. *Sem Rad Oncol*. 2017;27(4):350–357. doi:10.1016/j.semradonc.2017.04.002
- Culleton S, Jiang HY, Haddad CR, et al. Outcomes following definitive stereotactic body radiotherapy for patients with child-Pugh B or C hepatocellular carcinoma. *Radiother Oncol*. 2014;111(3):412–417. doi:10.1016/j.radonc.2014.05.002
- Feng M, Ben-Josef E. Radiation therapy for hepatocellular carcinoma. *Sem Rad Oncol*. 2011;21(4):271–277. doi:10.1016/j.semradonc.2011.05.002
- Ingold JA, Reed GB, Kaplan HS, et al. RADIATION HEPATITIS. *Am J Roentgenol Radium Ther Nucl Med*. 1965;93:200–208.
- Lambin P, Rios-Velazquez E, Leijenaar R, et al. Radiomics: extracting more information from medical images using advanced feature analysis. *Eur J Cancer*. 2012;48(4):441–446. doi:10.1016/j.ejca.2011.11.036
- Shen PC, Huang WY, Dai YH, et al. Radiomics-based predictive model of radiation-induced liver disease in hepatocellular carcinoma patients receiving stereo-tactic body radiotherapy. *Biomedicines*. 2022;10(3):597. doi:10.3390/biomedicines10030597
- Yoon JH, Lee JM, Yu MH, et al. Simultaneous evaluation of perfusion and morphology using GRASP MRI in hepatic fibrosis. *Eur Radiol*. 2022;32(1):34–45. doi:10.1007/s00330-021-08087-2
- Zhang JY, Liu MT, Qu Q, et al. Radiomics analysis of gadoxetic acid-enhanced MRI for evaluating vessels encapsulating tumour clusters in hepatocellular carcinoma. *Front Oncol*. 2024;14. doi:10.3389/fonc.2024.1422119
- Ma H, Wang L, Sun L, et al. Preoperative prediction of microvascular invasion in hepatocellular carcinoma from multi-sequence magnetic resonance imaging based on deep fusion representation learning. *IEEE J Biomed Health Inform*. 2025;29(5):3259–3271. doi:10.1109/JBHI.2024.3451331
- Chen BB, Hsu CY, Yu CW, et al. Hepatic necro-inflammation and elevated liver enzymes: evaluation with MRI perfusion imaging with gadoxetic acid in chronic hepatitis patients. *Clin Radiol*. 2014;69(5):473–480. doi:10.1016/j.crad.2013.12.003
- Haddad MM, Merrell KW, Hallemeier CL, et al. Stereotactic body radiation therapy of liver tumors: post-treatment appearances and evaluation of treatment response: a pictorial review. *Abdom Radiol*. 2016;41(10):2061–2077. doi:10.1007/s00261-016-0768-x
- Zhou YJ, Tang Y, Liu SJ, et al. Radiation-induced liver disease: beyond DNA damage. *Cell Cycle*. 2023;22(5):506–526. doi:10.1080/15384101.2022.2131163
- Coenegrachts K, Ghekiere J, Denolin V, et al. Perfusion maps of the whole liver based on high temporal and spatial resolution contrast-enhanced MRI (4D THRIVE): feasibility and initial results in focal liver lesions. *Eur J Radiol*. 2010;74(3):529–535. doi:10.1016/j.ejrad.2009.03.029
- Wu JW, Yu YC, Qu XL, et al. Optimization of hepatobiliary phase delay time of Gd-EOB-DTPA-enhanced magnetic resonance imaging for identification of hepatocellular carcinoma in patients with cirrhosis of different degrees of severity. *World J Gastroenterol*. 2018;24(3):415–423. doi:10.3748/wjg.v24.i3.415
- Yun TJ, Park CK, Kim TM, et al. Glioblastoma treated with concurrent radiation therapy and temozolomide chemotherapy: differentiation of true progression from pseudoprogression with quantitative dynamic contrast-enhanced MR imaging. *Radiology*. 2015;274(3):830–840. doi:10.1148/radiol.14132632
- Gawish RA, Samy EM, Aziz MM. Ferulic acid protects against gamma-radiation induced liver injury via regulating JAK/STAT/Nrf2 pathways. *Arch Biochem Biophys*. 2024;753:109895. doi:10.1016/j.abb.2024.109895
- Ye LF, Chaudhary KR, Zandkarimi F, et al. Radiation-induced lipid peroxidation triggers ferroptosis and synergizes with ferroptosis inducers. *ACS Chem Biol*. 2020;15(2):469–484. doi:10.1021/acscchembio.9b00939
- Xia TY, Zhou ZH, Meng XP, et al. Predicting microvascular invasion in hepatocellular carcinoma using CT-based radiomics model. *Radiology*. 2023;307(4). doi:10.1148/radiol.222729
- Ding WZ, Wang Z, Liu FY, et al. A hybrid machine learning model based on semantic information can optimize treatment decision for naive single 3-5-cm HCC patients. *Liver Cancer*. 2022;11(3):256–267. doi:10.1159/000522123
- Marrero JA, Kulik LM, Sirlin CB, et al. Diagnosis, staging, and management of hepatocellular carcinoma: 2018 practice guidance by the American association for the study of liver diseases. *Hepatology*. 2018;68(2):723–750. doi:10.1002/hep.29913
- Jang WI, Jo S, Moon JE, et al. The current evidence of intensity-modulated radiotherapy for hepatocellular carcinoma: a systematic review and meta-analysis. *Cancers*. 2023;15(20):4914. doi:10.3390/cancers15204914
- Su TS, Liang SX, Li LQ, et al. New staging model for radiation-based hepatocellular carcinoma treatment: a national multicenter study. *J Clin Transl Hepatol*. 2023;11(2):341–349. doi:10.14218/jct.2022.00002
- Pan CC, Kavanagh BD, Dawson LA, et al. Radiation-associated liver injury. *Inter J Radiation Oncol Biol Phys*. 2010;76(3):S94–100. doi:10.1016/j.ijrobp.2009.06.092.
- Xu Y, Lu L, Sun SH, et al. Effect of CT image acquisition parameters on diagnostic performance of radiomics in predicting malignancy of pulmonary nodules of different sizes. *Eur Radiol*. 2022;32(3):1517–1527. doi:10.1007/s00330-021-08274-1

34. Yang SX, Wu N, Zhang L, et al. Evaluation of the linear interpolation method in correcting the influence of slice thicknesses on radiomic feature values in solid pulmonary nodules: a prospective patient study. *Ann transl Med*. 2021;9. doi:10.21037/atm-20-2992
35. Song Y, Zhang J, Zhang YD, et al. FeAture explorer (FAE): a tool for developing and comparing radiomics models. *PLoS One*. 2020;15(8):e0237587. doi:10.1371/journal.pone.0237587
36. Huang FN, Shangguan W, Li QL, et al. Beyond prediction: an integrated post-hoc approach to interpret complex model in hydrometeorology. *Environ Modell Software*. 2023;167:105762. doi:10.1016/j.envsoft.2023.105762
37. Kim TH, Kim DY, Park JW, et al. Dose-volumetric parameters predicting radiation-induced hepatic toxicity in unresectable hepatocellular carcinoma patients treated with three-dimensional conformal radiotherapy. *Int J Radiat Oncol Biol Phys*. 2007;67(1):225–231. doi:10.1016/j.ijrobp.2006.08.015
38. Liang SX, Zhu XD, Xu ZY, et al. Radiation-induced liver disease in three-dimensional conformal radiation therapy for primary liver carcinoma: the risk factors and hepatic radiation tolerance. *Int J Radiat Oncol Biol Phys*. 2006;65(2):426–434. doi:10.1016/j.ijrobp.2005.12.031
39. Asakura H, Hashimoto T, Zenda S, et al. Analysis of dose-volume histogram parameters for radiation pneumonitis after definitive concurrent chemoradiotherapy for esophageal cancer. *Radiother Oncol*. 2010;95(2):240–244. doi:10.1016/j.radonc.2010.02.006
40. Liu MM, Ding CY, Li ZH, et al. Multiple exposures to low-dose ionizing radiation induced the initiation and progression of pro-atherosclerotic phenotypes in mice and vascular endothelial cell damage. *Sci Prog*. 2024;107(1). doi:10.1177/00368504241228668
41. Seidensticker M, Seidensticker R, Mohnike K, et al. Quantitative in vivo assessment of radiation injury of the liver using Gd-EOB-DTPA enhanced MRI: tolerance dose of small liver volumes. *Radiat Oncol*. 2011;6(1). doi:10.1186/1748-717x-6-40
42. Wu QY, Wang YD, Wei YX, et al. Development and validation of a nomogram for radiation-induced hepatic toxicity after intensity modulated radiotherapy for hepatocellular carcinoma: a retrospective study. *Japanese J Clin Oncol*. 2024;54(6):699–707. doi:10.1093/jjco/hyae024
43. Su TS, Luo R, Liang P, et al. A prospective cohort study of hepatic toxicity after stereotactic body radiation therapy for hepatocellular carcinoma. *Radiother Oncol*. 2018;129(1):136–142. doi:10.1016/j.radonc.2018.02.031
44. Velec M, Haddad CR, Craig T, et al. Predictors of liver toxicity following stereotactic body radiation therapy for hepatocellular carcinoma. *Int J Radiat Oncol Biol Phys*. 2017;97(5):939–946. doi:10.1016/j.ijrobp.2017.01.221
45. Gutin I. In BMI we trust: reframing the body mass index as a measure of health. *Social Theory & Health: STH*. 2018;16(3):256–271. doi:10.1057/s41285-017-0055-0
46. Mueller C, Compher C, Ellen DM, et al. A.S.P.E.N. Clinical guidelines nutrition screening, assessment, and intervention in adults. *J Parenteral Enteral Nutr*. 2011;35(1):16–24. doi:10.1177/0148607110389335
47. Abe M, Akbar F, Matsuura B, et al. Defective antigen-presenting capacity of murine dendritic cells during starvation. *Nutrition*. 2003;19(3):265–269. doi:10.1016/s0899-9007(02)00854-7
48. Kloeckner R, Otto G, Biesterfeld S, et al. MDCT versus MRI assessment of tumor response after transarterial chemoembolization for the treatment of hepatocellular carcinoma. *Cardiovasc Intervent Radiol*. 2010;33(3):532–540. doi:10.1007/s00270-009-9728-y
49. Zheng J, Du PZ, Yang C, et al. DCE-MRI-based radiomics in predicting angiopoietin-2 expression in hepatocellular carcinoma. *Abdom Radiol*. 2023;48(11):3343–3352. doi:10.1007/s00261-023-04007-8
50. Zhou Y, Zhou GF, Zhang JL, et al. DCE-MRI based radiomics nomogram for preoperatively differentiating combined hepatocellular-cholangiocarcinoma from mass-forming intrahepatic cholangiocarcinoma. *Eur Radiol*. 2022;32(7):5004–5015. doi:10.1007/s00330-022-08548-2
51. Xiao BH, Wang PG, Zhao YR, et al. Nasopharyngeal carcinoma perfusion MRI Comparison of arterial spin labeling and dynamic contrast-enhanced MRI. *Medicine*. 2020;99(22):e20503. doi:10.1097/md.00000000000020503
52. Kim KA, Kim MJ, Jeon HM, et al. Prediction of microvascular invasion of hepatocellular carcinoma: usefulness of peritumoral hypointensity seen on gadoxetate disodium-enhanced hepatobiliary phase images. *J Magn Reson Imaging*. 2012;35(3):629–634. doi:10.1002/jmri.22876
53. Choi BI, Lee KH, Han JK, et al. Hepatic arteriportal shunts: dynamic CT and MR features. *Korean J Radiol*. 2002;3(1):1–15. doi:10.3348/kjr.2002.3.1.1
54. Huang XL, Long LL, Wei JQ, et al. Radiomics for diagnosis of dual-phenotype hepatocellular carcinoma using Gd-EOB-DTPA-enhanced MRI and patient prognosis. *J Cancer Res Clin Oncol*. 2019;145(12):2995–3003. doi:10.1007/s00432-019-03062-3
55. Kumar V, Gu YH, Basu S, et al. Radiomics: the process and the challenges. *Magnetic Resonance Imaging*. 2012;30(9):1234–1248. doi:10.1016/j.mri.2012.06.010
56. Pantic JP, Vucevic D, Radosavljevic T, et al. Machine learning approaches to detect hepatocyte chromatin alterations from iron oxide nanoparticle exposure. *Sci Rep*. 2024;14. doi:10.1038/s41598-024-70559-4
57. Martins SN, Paiva C, Azevedo RS, et al. Histological grading of hepatocellular carcinoma-a systematic review of literature. *Front Med*. 2017;4. doi:10.3389/fmed.2017.00193
58. Tong C, Xu X, Liu C, et al. Assessment of liver volume variation to evaluate liver function. *Front Med*. 2012;6(4):421–427. doi:10.1007/s11684-012-0223-5
59. Lauth WW. Regulatory processes interacting to maintain hepatic blood flow constancy: vascular compliance, hepatic arterial buffer response, hepatorenal reflex, liver regeneration, escape from vasoconstriction. *Hepatol Res*. 2007;37(11):891–903. doi:10.1111/j.1872-034X.2007.00148.x
60. Bera K, Braman N, Gupta A, et al. Predicting cancer outcomes with radiomics and artificial intelligence in radiology. *Nat Rev Clin Oncol*. 2022;19(2):132–146. doi:10.1038/s41571-021-00560-7
61. Pinker K, Chin J, Melsaether AN, et al. Precision medicine and radiogenomics in breast cancer: new approaches toward diagnosis and treatment. *Radiology*. 2018;287(3):732–747. doi:10.1148/radiol.2018172171
62. Ibragimov B, Toesca DAS, Chang DT, et al. Deep learning for identification of critical regions associated with toxicities after liver stereotactic body radiation therapy. *Med Phys*. 2020;47(8):3721–3731. doi:10.1002/mp.14235
63. Sorkhi AG, Pirgazi J, Ghasemi V. A hybrid feature extraction scheme for efficient malonylation site prediction. *Sci Rep*. 2022;12(1). doi:10.1038/s41598-022-08555-9
64. Giannini EG, Bucci L, Garuti F, et al. Patients with advanced hepatocellular carcinoma need a personalized management: a lesson from clinical practice. *Hepatology*. 2018;67(5):1784–1796. doi:10.1002/hep.29668
65. Zhao TM, Mao LH, Yu ZH, et al. Therapeutic potential of bicyclol in liver diseases: lessons from a synthetic drug based on herbal derivative in traditional Chinese medicine. *Int Immunopharmacol*. 2021;91:107308. doi:10.1016/j.intimp.2020.107308

66. Zhang RJ, Zhou HM, Lu HY, et al. Radiotherapy plus anti-PD1 versus radiotherapy for hepatic toxicity in patients with hepatocellular carcinoma. *Radiat Oncol.* **2023**;18(1). doi:10.1186/s13014-023-02309-1
67. Li GX, Shu B, Zheng ZZ, et al. Safety and efficacy of radiotherapy combined with lenvatinib plus PD-1 inhibitors as neo-adjuvant therapy in hepatocellular carcinoma with portal vein thrombus: protocol of an open-label, single-arm, prospective, multi-center phase I trial. *Front Oncol.* **2022**;12. doi:10.3389/fonc.2022.1051916

Journal of Hepatocellular Carcinoma

Dovepress
Taylor & Francis Group

Publish your work in this journal

The Journal of Hepatocellular Carcinoma is an international, peer-reviewed, open access journal that offers a platform for the dissemination and study of clinical, translational and basic research findings in this rapidly developing field. Development in areas including, but not limited to, epidemiology, vaccination, hepatitis therapy, pathology and molecular tumor classification and prognostication are all considered for publication. The manuscript management system is completely online and includes a very quick and fair peer-review system, which is all easy to use. Visit <http://www.dovepress.com/testimonials.php> to read real quotes from published authors.

Submit your manuscript here: <https://www.dovepress.com/journal-of-hepatocellular-carcinoma-journal>